Math. Model. Nat. Phenom. 18 (2023) 15
https://doi.org/10.1051/mmnp/2023011

Mathematical Modelling of Natural Phenomena
www.mmnp-journal.org

INTERACTION BETWEEN CROWDING AND GROWTH IN TUMOURS WITH STEM CELLS: CONCEPTUAL MATHEMATICAL MODELLING

Luca Meacci[1,*] and Mario Primicerio[2]

Abstract. This research paper proposes and discusses a conceptual modelling of both growth of tumours in presence of immortal multipotent cancer stem cells (CSCs) and of several lineages of differentiated tumour cells (CCs). The replication of CSCs is assumed symmetric or asymmetric with a prescribed mean ratio and mitosis and apoptosis are taken into account for the CCs aging. Replication can be hindered by the local crowding of the cells in the vicinity of the mother cell. The model is implemented in the framework of 3D cellular automata (CA) whose dynamics is governed by stochastic rules. Some simulations are displayed showing the growth of a tumour and the fractions of different lineages and age classes of CCs. Then, an approach that considers the same dynamics of aging, replication, and apoptosis, but with the aim to study the time evolution of the fractions of the different lineages and age classes of cells averaged over the total volume is presented. The dynamics is governed by a system of ordinary differential equations (ODEs), hence by deterministic rules. Numerical simulations of the solution of this system show qualitative similarity with the CA results, although the crowding effect is no longer a local effect, but also averaged over the total volume. The Appendix provides the proof of the mathematical well-posedness of this model in a general framework.

Mathematics Subject Classification. 92-08, 92C50, 68Q80, 35Q92.

Received December 30, 2021. Accepted February 22, 2023.

1. Introduction

The growth of tumours in presence of stem cells has been the object of an increasing number of papers on theoretical and experimental research (see *e.g.* [2, 8–10, 21, 22, 27, 32, 34, 35, 42]).

The mathematical modeling of such a phenomenon frequently uses methods of population dynamics. The basic idea consists in studying the evolution and mutual interactions of two sub-populations of malignant cells, namely cancer stem cells (CSCs) and differentiated cancer cells (CCs). The former are assumed to be immortal and capable of proliferating indefinitely; their mitosis can be asymmetric (*i.e.*, producing one CSC and one

Keywords and phrases: Cancer stem cells, mathematical modeling, cellular automata, age-dependent cell replication.

[1] Instituto de Ciências Matemáticas e de Computação, Universidade de São Paulo, Av. Trab. São Carlense 400, São Carlos (SP), 13566-590 Brazil.
[2] Dipartimento di Matematica "U. Dini", Università degli Studi di Firenze, Viale Morgagni, 67/a - 50134 Firenze (FI), Italy.

* Corresponding author: luca.meacci@gmail.com

CC) or symmetric (*i.e.*, producing two cells of the same type, either CSCs, or CCs).[1] Differentiated cells CCs can belong to different lineages, in which the usual process of age progression, replication, and apoptosis takes place. The replication of CCs is always symmetric, *i.e.*, it produces two newborn CCs. There is an extensive bibliography in this area ([3, 4, 13, 15, 16, 28, 29, 40, 41, 43, 44] and the references quoted therein).

In [12] it has been suggested that an important role in the replication of cells might be played by the local "crowding" of cells. From a mathematical point of view, it corresponds to assuming the proliferation rate of each cell may depend on its position, since it can be hindered by the presence of other cells in its vicinity. This fact has been incorporated in different classes of models, namely (i) the classified as "agent-based" ones [1] *i.e.*, considering the evolution of each cell, using computer simulations and/or cellular automata (CA) methods ([17, 23–25, 30, 31, 33, 38], and the reviews [6, 26, 36]), (ii) those that introduce partial differential equations and integral terms to take into account the space-dependence of the cellular dynamics [7, 14, 19, 20, 38], and (iii) models that are "mean field approximations" of the dynamics of individual cells, taking the averaged fraction of each sub-population as unknown and modifying the compartmental schemes of the population dynamics multiplying the proliferation rate by a monotonic function of the fraction of cells and decreasing to zero when all available space is filled by other cells [5, 24, 25].

In general, the effect of aging was not taken into account in the cited literature (although in some individual based models, *e.g.* [12], the replication rate is assumed to decrease after every mitosis) and the possibility of multiple lineages of differentiated cells was neglected. Moreover, the CA simulations are always two-dimensional.

The introduction of "crowding" effect enables descriptions of the tumour growth paradox, which consists of an accelerated tumour growth as a consequence of cytotoxic treatment [12, 18, 45, 46].

Section 2 introduces a 3D model with cellular automata whose evolution is governed by stochastic rules. Several lineages of CCs can be present and each cell is characterized by a different degree of maturity (newborn, juvenile, adult, and senescent), hence by different probabilities for dormancy, aging, replication, and apoptosis.[2] The crowding effect is also taken into account. In a generalized version of the model, all probabilities can be supposed to be space-dependent and variable in time; also the case of a proliferation rate decreasing at each cycle (see [13]) could be taken into account. Section 2.1 discusses models with only one lineage of differentiated cancer cells and Section 2.2 addresses some simulations that evidence the tumour growth paradox. Section 2.3 focuses on different lineages and some simulations, also considering the case of a specific treatment on one lineage. The model is conceptual; the values of the parameters are chosen in a speculative way and thus the numerical simulation does not provide experimental-based results, but a correct qualitative insight in this complex phenomenon. In particular, the results highlight the tumour paradox, offering suggestions towards optimizing the strategy of cytotoxic treatment.

Section 3 presents a deterministic model that describes the growth of the tumour in terms of total number of cells of each type and lineage in the domain under consideration. The age distribution of the CCs is assumed continuous; consequently, its evolution is governed by a first-order partial differential equation (PDE) (Sect. 3.1). The crowding effect is no longer considered a local effect but it is averaged over the whole region in the typical spirit of mean field approximations. The mathematical well-posedness of the model is proved in the Appendix A. Section 3.2 provides some numerical results of the model after its reduction to a system of ordinary differential equations (ODEs), as usual in compartmental models. Global information on the growth of the tumour was obtained, confirming the tumour growth paradox. Section 3.3 presents a short comparison between CA models and models based on differential equations.

Finally, Section 4 is devoted to conclusions.

[1] For simplicity, in the sequel, we confine to the case in which symmetric mitosis produces two new CSC (see [17]). However, the model can be easily adapted to cover both types of symmetric mitosis.

[2] In the following the terms aging, dormancy, replication, and apoptosis denote, respectively, the progressive change of the physiological mechanisms in the cell cycle, the possibility of the cell cycles being temporarily interrupted and the cell entering a quiescent state, the conclusion of the cycle leading to mitosis, and the programmed death of the cell.

2. Cellular automata modelling

2.1. The basic model

To illustrate the model, we first assume to neglect the lineages, *i.e.*, we consider the case in which there exists only one lineage of CCs.

Let us suppose the cells live in a $50 \times 50 \times 50$ cubic lattice. At each time step, each site in the lattice can be either vacant (white), or occupied by a CSC (black), or by a CC, which may be newborn, juvenile, adult, or senescent, denoted with blue, green, yellow and red colors, respectively.

Starting from a given time t_k, the following rules are applied towards updating the system:

1. Each CC may undergo **apoptosis** in the following time interval with probability μ_1, μ_2, μ_3, μ_4 (where, here and henceforth, indexes 1, 2, 3, and 4 refer to newborn, juvenile, adult, and senescent cells, respectively). The corresponding site becomes vacant, illustrated by white color.
2. Each cell may undergo **dormancy** with probability δ in case of CSC, or δ_1, δ_2, δ_3, δ_4 for the CCs (according to its age class). The cell remains in the same state (*i.e.*, it does not change color) and does not replicate in the time step (t_k, t_{k+1}).
3. The probability of **replication** of each surviving and nondormant cell is equal to ρ in case of CSC, or ρ_1, ρ_2, ρ_3, ρ_4 in case of CCs (according to its age class) multiplied by a **crowding factor** given by the fraction θ of the vacant sites[3] in a neighborhood of the mother cell (see Rems. 2.2 and 2.3).
4. The **mitosis** of a CC is always symmetric and modelled as follows: the site of the mother cell and one of the vacant sites of the neighbourhood randomly chosen (with a uniform distribution) become pale blue. In the case of a CSC, a constant $d \in [0, 1]$ can be defined and provides the ratio of the asymmetric mitosis (producing one CSC and one CC). Therefore, a daughter CSC appears in its neighbourhood with probability $(1 - d)$. Otherwise, the new cell is a pale blue CC.
5. Each surviving and nondormant CC that did not replicate may change its state (from newborn to juvenile, form juvenile to adult, from adult to senescent) with probabilities p_1, p_2, p_3.

Remark 2.1. The model does not include the mechanism of de-differentiation *i.e.*, the effect that a CC cell can gain CSC behavior. This process was not incorporated in our simulations; however, such an effect might increase the growth paradox. This effect and the occurrence of a "differentiated symmetric mitosis" (*i.e.*, a CSC originating two CCs) will be considered in future studies.

Remark 2.2. In the simplest case, the neighborhood of the would-be mother cell in which the newborn cell can be located is a cubic shell of $3 \times 3 \times 3$ lattice sites centered in the site of the replicating cell. A possible generalization might consist in considering the $5 \times 5 \times 5$ adjacent cubic shell when no vacant sites are present in the $3 \times 3 \times 3$ shell, and so on. In this case, in each step the probability of replication is reduced, because energy is spent in the displacement of the nearest cells. In the sequel, we will use the $3 \times 3 \times 3$ shell.

Remark 2.3. Regarding the definition of the crowding effect, instead of multiplying ρ by fraction θ of the vacant sites, it can be multiplied by a chosen function $G(\theta)$ belonging to $[0, 1]$, with $G(0) = 0$ and $G(1) = 1$.

Remark 2.4. It is evident that a single simulation made through CA is not representative, due to the stochastic character of the method. Therefore the plots of Figures 3–9 represent the average over 10 simulations. To evaluate the order of variability, the Figures 3, 5, and 6 display the standard deviation around the average of the results.

Starting from a specific initial condition, the CA model runs through all positions of the lattice following a geometric order (otherwise, a random order can be used; see Rem. 2.5).

For each unit of time and, based on the presence or absence of a certain type of cell and its state with respect to the age progression, the algorithm decides on how to update the system. Figure 1 shows a flowchart that implements the aforementioned hypotheses. The algorithm makes nondeterministic decisions, but responds to

[3] $\theta = \nu_v/\nu$, being ν_v the number of the vacant sites in the chosen neighborhood and ν is the total number of sites in the neighborhood.

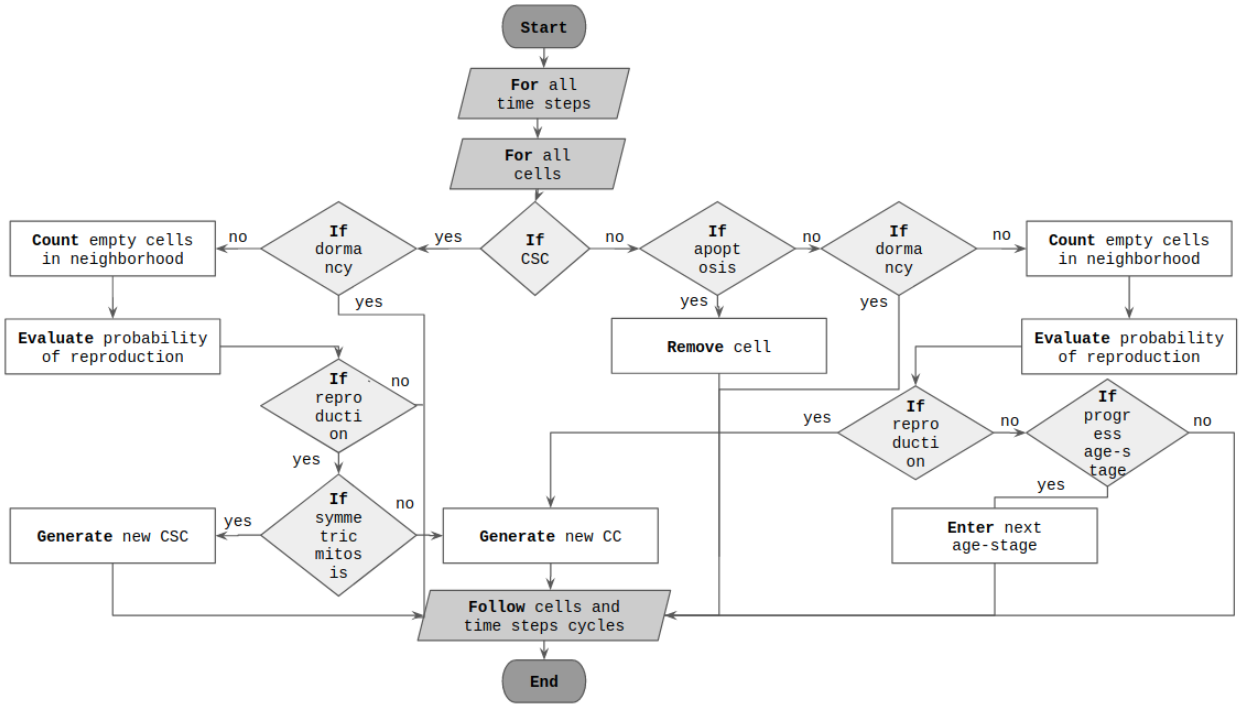

FIGURE 1. Flowchart of CA algorithm concerning the model for the tumour progression with cancer stem cells and one lineage of cancer cells.

probabilities, thus having a certain degree of randomness. The running of a sufficient number of simulations shows on average, the overall behaviour tends to a specific situation with respect to a certain parameter setup. The usefulness of an approach based on cellular automata is its possibility of prescription of local processes and interactions (on single cells) and study the collective behaviour of the system over time *i.e.*, in our case, the tumour progression.

By following the previous instructions, the model can predict and visualize the three-dimensional evolution of tumour growth, retaining details of the characterization of each single cell with respect to type and age.

According to the panels in Figure 2, starting from a condition of a small central nucleus of $3 \times 3 \times 3$ CSCs (see panel (a)), it is possible to study the evolution of the tumoral tissue during a certain time. Panel (b) shows the visualization by age class after a certain time progression ($t = 50$) when the parameters setup is chosen as in Table 1. To simulate tests with different choices of the parameters, the reader can refer to the Matlab code freely accessible in the GitHub repository https://github.com/LucaMeacci/ConceptualCSCmathmodellingForCancers.

2.2. Tumour growth paradox

This conceptual model can perform simulations to illustrate the qualitative behaviour of the system. Indeed, the choice of parameters according to only laboratory experiments would enable a quantitative validation of the model.

Firstly, the tumour response will be evaluated against a hypothetical medical treatment. Therefore, let us mimic the effect of the treatment by an increase of the mortality of the CCs; a parameter ξ is introduced and the new mortality for each cell age class j is assumed to be $\xi\,\mu_j$.

We also mention some premises. The time unit can be arbitrarily chosen as long as the parameters are adjusted. Indeed, parameters μ, ρ, and p represent the probability a given event (apoptosis, mitosis, or age

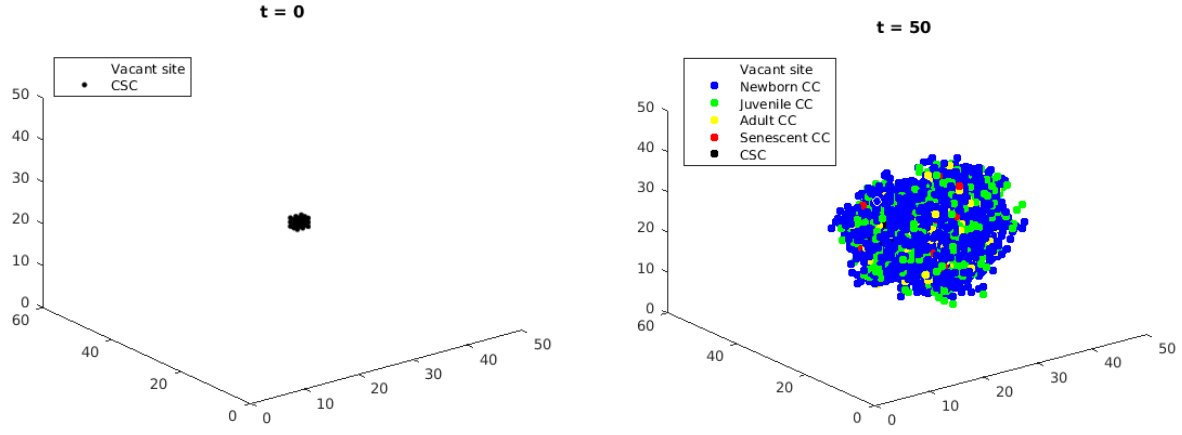

(**a**) (**b**)

FIGURE 2. Progression of the tumour tissue using the computational model of cellular automata. The panel (a) shows the initial condition of a $3 \times 3 \times 3$ CSCs nucleus in the center. The panel (b) displays the prediction of tumour progression after a certain time ($t = 50$) by displaying the respective age cell classes. The parameters setup can be found in Table 1. To run similar simulations, a Matlab code is published in the public GitHub repository https://github.com/LucaMeacci/ConceptualCSCmathmodellingForCancers.

TABLE 1. Setup of parameters for the CA simulations.

CSC	Newborn CC	Juvenile CC	Adult CC	Senescent CC
$\rho = 1$	$\rho_1 = 0.7$	$\rho_2 = 0.9$	$\rho_3 = 1.0$	$\rho_4 = 0.5$
–	$\mu_1 = 0.30$	$\mu_2 = 0.30$	$\mu_3 = 0.30$	$\mu_4 = 0.48$
–	$p_1 = 1$	$p_2 = 1$	$p_3 = 1$	–
$\delta = 0$	$\delta_1 = 0$	$\delta_2 = 0$	$\delta_3 = 0$	$\delta_4 = 0$
$d = 0.8$	–	–	–	–

progression) occurs in the time unit chosen and depend on the choice of the time step. $\rho = 1$ was chosen so that the time step corresponds to the average cycle duration of a CSC in absence of dormancy. In accordance with the choice, we list the setup of parameters in Table 1 for the case of one lineage of CCs. The values of dormancy (δ, δ_1, δ_2, δ_3, δ_4) that simply slow down the process are zero. In this case, no differentiation in lineages is assumed.

27 CSCs were arranged in a cube in the lattice center as the initial condition for the study of the evolution of the system with respect to mortality variation. Figure 3 displays the graphs of the fraction of tumour cells (number of CSCs and CCs over all available spaces in the lattice under consideration) in the lattice, modifying the mortality (starting at $t = 0$) by different values of the parameter ξ.

The results appear to be counter-intuitive at first glance. After certain time, the tumour volume turns out to be greater as mortality increases. This occurrence means that a more aggressive treatment would not benefit the patient. The phenomenon is called the "tumour growth paradox" because an increased mortality of the CCs may cause a faster growth of the tumour. Nevertheless, the model helps to understand why this situation can be expected under our assumptions. Let us consider the two cases with $\xi = 1.0$ and $\xi = 1.5$ and focus on the evolution of CSCs and CCs for the age groups. Figure 4 displays the corresponding graphs.

CSCs are not affected by the increase in mortality; on the contrary, when $\xi = 1.5$, they are significantly become more numerous than in the previous simulation. From the point of view of the tumour progression,

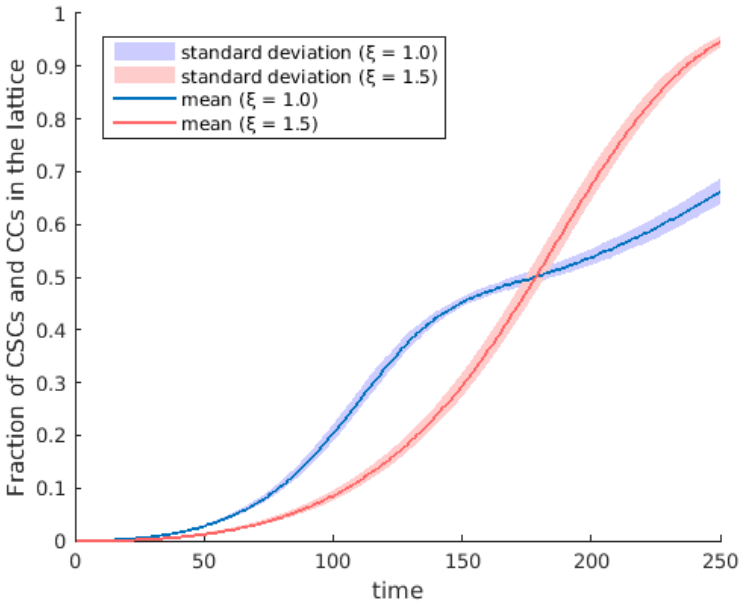

FIGURE 3. Quantitative evolution of the fraction of tumoral cells (number of CSCs and CCs over all the available spaces in the lattice) with respect to the mortality variation, according to the CA model. At the starting time, 27 CSCs are placed in the lattice center. The parameters setup is listed in Table 1. The values are given by the average over 10 simulations and the standard deviation is displayed in the graphs.

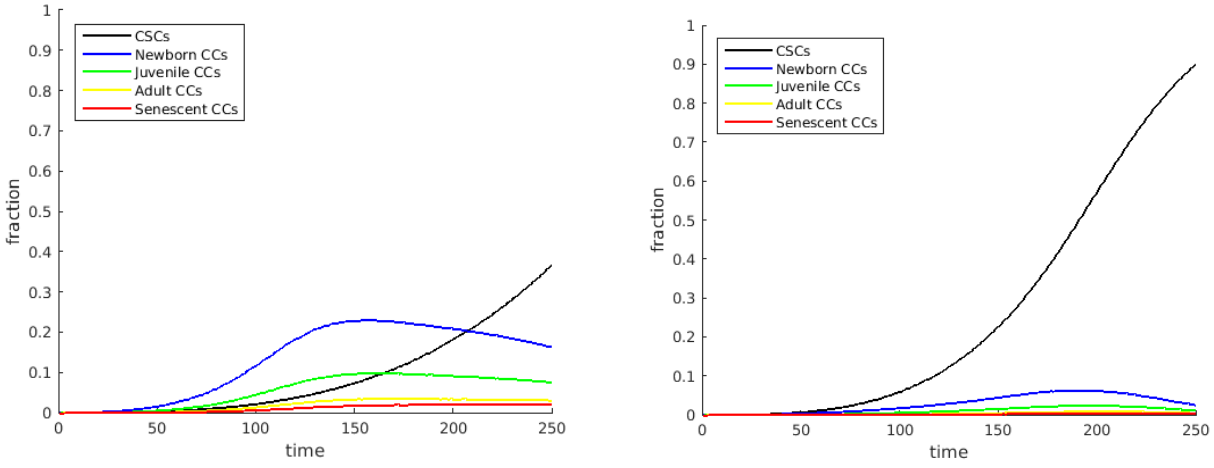

FIGURE 4. Quantitative evolution of the lattice fraction of CSCs and CCs divided into age classes. The case (a) corresponds to a mortality value induced by $\xi = 1.0$, while the case (b) results from $\xi = 1.5$. The simulation is the same of Figure 3.

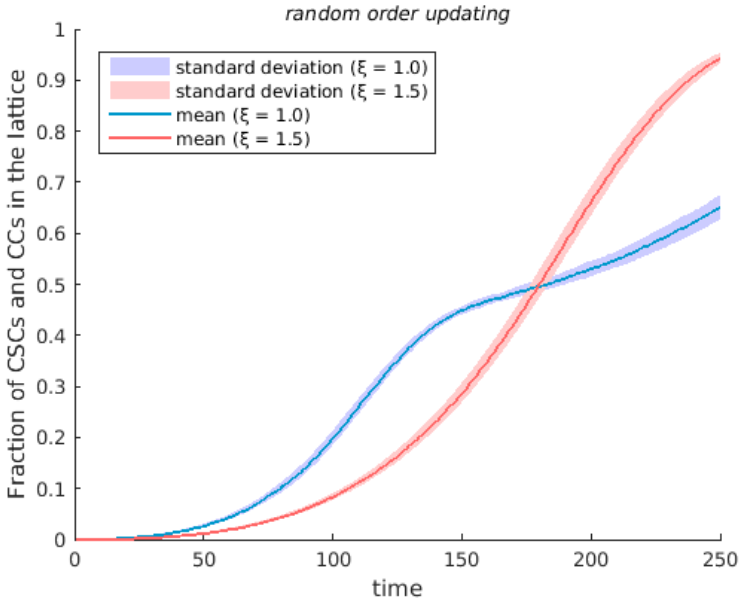

FIGURE 5. Quantitative evolution of the fraction of tumoral cells (number of CSCs and CCs over all the available spaces in the lattice) with respect to the mortality variation, using the CA model with a lattice random order of updating (instead of geometric sequential order). The initial conditions and the setup of parameters are the same of the simulation of Figure 3. The values are given by the average over 10 simulations and the standard deviation is displayed in the graphs.

in this case, therefore the CSCs (more aggressive and able to reproduce) have more free space and freedom of growth in comparison with $\xi = 1.0$. In a certain sense, when the mortality of the CCs is lower, they compete with CSCs for space and resources, thus reducing their proliferation.

Remark 2.5. As stated in Section 2.1, the updating of the state of the lattice model at each time step is made in sequential geometric order. In Figure 5 it is shown that using a different criterion (*e.g.*, random order) for the case simulated in Figure 3 the difference is negligible.

2.3. The case of several lineages of CCs

We can proceed with a further step forward. Although common characteristics and properties are usually clustered into two types of cancerous cells, namely ordinary or stem, the fact that differentiated cancer cells CCs belong to different lineages and their heterogeneity can play a significant role in the evolution of the tumour must be taken into account in some cases.

Let m be the number of different lineages, meaning there exist m positive constants d^1, d^2, ..., d^m such that d^j represents the fraction of asymmetric mitosis, resulting in cells of the jth lineage. Since $d = \sum d^i$, it should be < 1. In the CA model, the replication of a CSC has probability $1 - d$ of producing a new CSC and a probability d^j of producing a CC of the jth lineage. Such a feature enables the differentiation of parameters on the basis of the lineage. As an example, a CC of a certain lineage may assume a different apoptosis behavior or proliferation rate compared with a CC belonging to another lineage. Specifically, the following simulations consider the generation of 3 lineages, each of them characterized by certain values of the parameters, as shown in Table 2. Clearly, lineage 1 is the most aggressive of all lineages.

TABLE 2. Update of the setup of parameters concerning CCs differentiation in cells lineages for CA simulations. In the variables, the subscript stands for the age and the superscript stands for the lineage.

Lineage 1	Lineage 2	Lineage 3
$d^1 = 0.2$	$d^2 = 0.3$	$d^3 = 0.3$
$\rho_1^1 = 0.7$	$\rho_1^2 = 0.6$	$\rho_1^3 = 0.5$
$\rho_2^1 = 0.9$	$\rho_2^2 = 0.8$	$\rho_2^3 = 0.7$
$\rho_3^1 = 1.0$	$\rho_3^2 = 0.9$	$\rho_3^3 = 0.8$
$\rho_4^1 = 0.5$	$\rho_4^2 = 0.4$	$\rho_4^3 = 0.3$
$\mu_1^1 = 0.30$	$\mu_1^2 = 0.33$	$\mu_1^3 = 0.33$
$\mu_2^1 = 0.30$	$\mu_2^2 = 0.33$	$\mu_2^3 = 0.33$
$\mu_3^1 = 0.30$	$\mu_3^2 = 0.33$	$\mu_3^3 = 0.33$
$\mu_4^1 = 0.48$	$\mu_4^2 = 0.50$	$\mu_4^3 = 0.50$

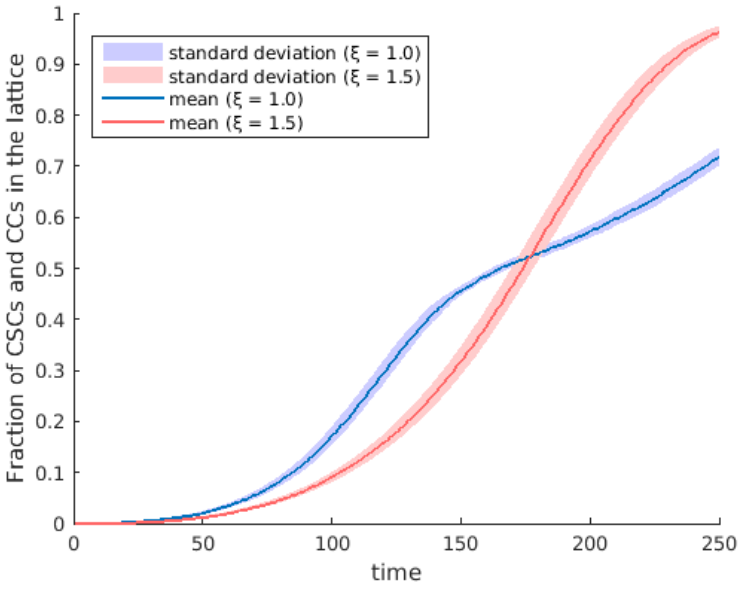

FIGURE 6. Quantitative evolution of the fraction of tumoral cells (CSCs and CCs) according to the CA model and the cell differentiation for different ξ. The initial condition is the same shown in panel (a) in Figure 2 and the parameters setup is provided in Tables 1 and 2 for the CSCs and for the 3 lineages of CCs, respectively. The values are given by the average over 10 simulations and the standard deviation is displayed in the graphs.

Each lineage may differ to some extent with respect to certain characteristics. From the model point of view, such a possibility can be translated with a parameters setup, when the values significantly differ from one lineage to another. We suppose to consider the previous configuration of the parameters for the CSCs as in Table 1 but, moreover, to differentiate by lineage CCs we set the other ones as in Table 2.

Also in this case with the generation of different lineages of CCs, if we mimic the cytotoxic treatment modifying the mortality (starting at $t = 0$) by tuning the parameter ξ, we can observe the development of the tumour growth paradox. Figure 6 shows the graphs of the fraction of CSCs and CCs in the lattice over time. At $t = 0$, the simulation starts with a central nucleus of $3 \times 3 \times 3$ CSCs and at the final time, the tumour volume is clearly bigger when $\xi = 1.5$ in comparison with $\xi = 1.0$.

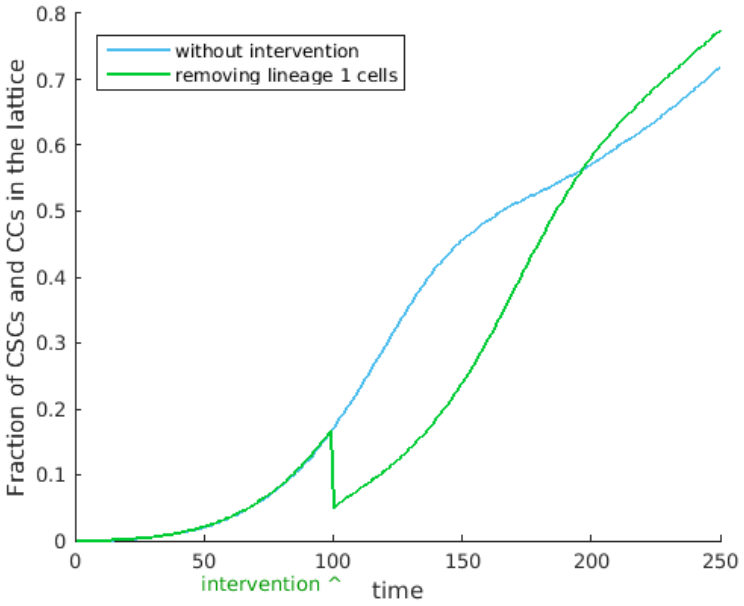

FIGURE 7. Quantitative evolution of the fraction of tumoral cells (CSCs and CCs), with no intervention and with removal of the CCs of lineage 1 at time $t = 100$. The initial condition is the same illustrated in Figure 2 and the parameters setup is provided in Tables 1 and 2 for the CSCs and for the 3 lineages of CCs, respectively.

The level of detail of the model allows us to intervene with specificity in order to simulate the strategies to combat the disease. Analogously to the previous study, we can hypothesize on a model medical treatment to reduce the cancer cells. The further assumption is to choose an intervention time for eliminating the CCs of a specific lineage, *i.e.*, number 1 in the subsequent simulations. The algorithm is instructed to completely remove the CCs of the first lineage at time $t = 100$. Assuming to mimic in this way the treatment, we remark that no further mortality modification will be applied during the simulation; therefore, $\xi = 1.0$. Figure 7 shows the time evolution of the fraction of number of tumoral cells (CSCs and CCs) over the spaces available in the lattice with and without this kind of intervention.

The sudden decrease in tumour volume is evident in the proximity of the intervention. Nonetheless, once again, a nonintuitive trend appears, showing the removal of a greater number of CCs (of lineage 1) is unfavorable for the progression of the disease.

We can analyze what happened at the level of age classes and lineages in the two cases. The respective behaviours are plotted in Figure 8.

Once again, such a nonintuitive conclusion can be justified. Due to the particular evolutionary characteristics of lineage 1, before the intervention time, the CCs of the first lineage turn out to be in the majority. Their removal facilitates the proliferation of CSCs which, finding more space available, accelerates the global growth of the tumour volume.

More complex scenarios can be explored, leading to similar conclusions. For instance, the apoptosis probability can be reduced only within a certain time interval to model a temporarily limited treatment. Moreover, many drugs used in oncology are mitotic inhibitors, *e.g.*, they aim to reduce cellular reproduction. Maintaining the same previous configuration and the setup in Table 2, we show corresponding examples of tumour growth paradoxical behaviour. Panel (a) in Figure 9 displays a comparison of the spontaneous evolution of the tumour with the application of a 50% increase in the mortality of all age stages of the cell lineage 1 in time interval

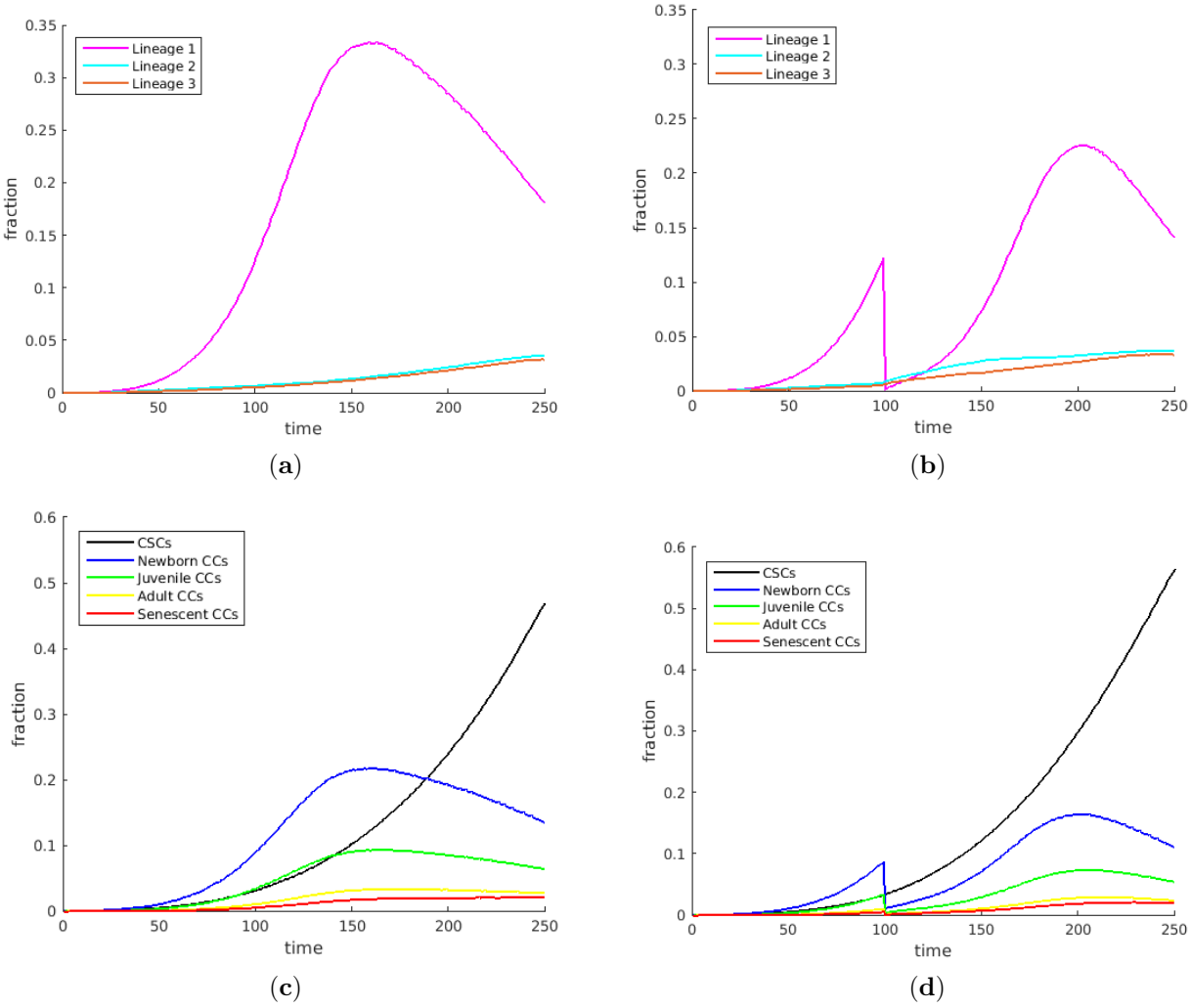

FIGURE 8. Quantitative progression of the tumour (fraction of CSCs and CCs over the lattice spaces) displayed according to the lineages (panel (a) without intervention and panel (b) considering $t = 100$ as removal time) and divided into age classes (panels (c) and (d) without and with the treatment). The simulation is the same of Figure 7.

$[100, 130]$. On the other case, Panel (b) shows a simulation of the drug-induced mitotic inhibition decreasing 50% of the reproduction parameters for the entire set of cells of lineage 1 within time interval $[60, 90]$.

Remark 2.6. The tumour heterogeneity is thoroughly documented as a pivotal factor in the fighting of cancer [37]. The heterogeneous population of the cancer cells undergoes a continual evolution with different patterns of treatment sensitivity. Our simulations showed an arbitrary differentiation of the treatment response for a specific lineage.

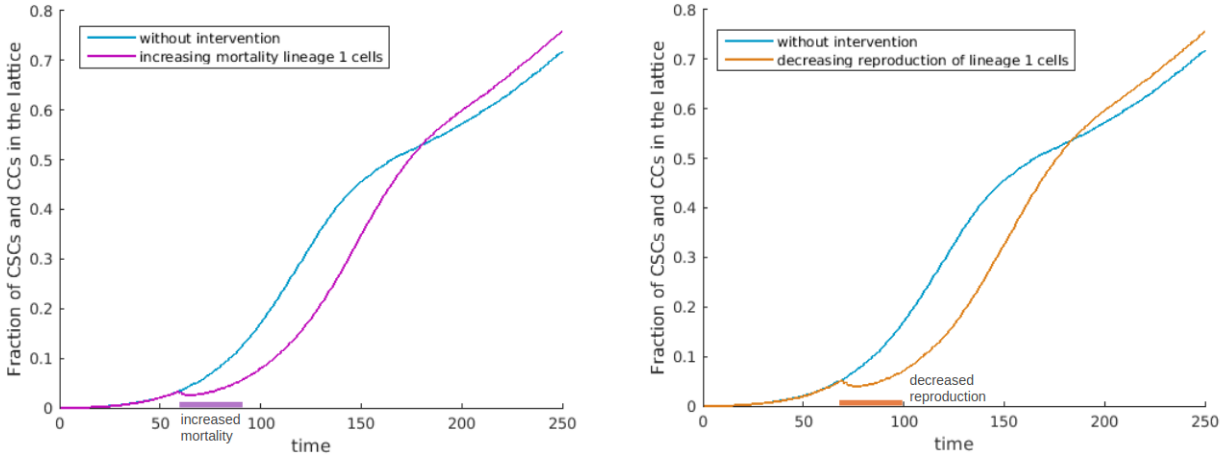

FIGURE 9. Quantitative evolution of the fraction of the number of CSCs and CCs over the lattice spaces. Treatments are simulated: cell lineage 1 assumes the mortality parameters increased of 50% for $t \in [100, 130]$ (in panel (a)) and reproduction parameters decreased of 50% for $t \in [60, 90]$ (in panel b)). We refer to the same initial condition and parameters setup described in the caption of Figure 7 .

3. Modelling based on differential equations

This Section describes the growth of the tumour in terms of the total number of cells in the region under consideration. Therefore, the space dependence of the fractions of both CSCs and CCs is not considered, but we average such fractions over the entire region. Indeed, the approach will lead to a loss of the individual-based description of the phenomenon displayed in Section 2.

3.1. From a PDE model to a compartmental system

Specifically, the number of the CSCs and of the M lineages of CCs was defined by $U(t)$, $V^1(t)$, $V^2(t)$, ..., $V^M(t)$ in the region and the existence of numbers d^i $(i = 1, 2, \ldots, M)$ was assumed such that if $d = \sum_i d^i < 1$, then $1 - d$ represents the fraction of symmetric replication of CSC (*i.e.* mitosis originating 2 CSCs), whereas each d^i is the fraction of the mitosis of CSC that originates a CC of the ith lineage.

Towards incorporating the effect of competition for space ("crowding effect"), the mitosis rate of the cells will be multiplied by a function F, depending on the total number of cells, and being zero when the cell fraction reaches a maximum carrying capacity, in this case set to 1 for simplicity. The volumes of all cells are implicitely assumed equal so that, with a little abuse of notation, quantities $U(t)$, $V^1(t)$, $V^2(t)$, ..., $V^M(t)$ will represent the fractions of the total volume of the region under consideration occupied by both CSC and the M lineages of CCs.

Therefore, the time evolution of the number of CSCs in the region is governed by the following equation:

$$\dot{U}(t) = \rho\,(1 - d)\,U(t)\,F(P(t)), \quad U(0) = U_0\ , \tag{3.1}$$

where

$$P(t) = U(t) + V(t), \quad V(t) = \sum_i V^i(t)\ , \tag{3.2}$$

ρ is the replication rate of CSC and F is a monotonic decreasing function such that $F(0) = 1$ and $F(1) = 0$.

Age distribution functions $v^i(a,t)$, where a denotes the "age" of the cell and for any $t > 0$ and $0 < a_1 < a_2$, $\int_{a_1}^{a_2} v^i(a,t)da$ is the number of cells of the i-th lineage whose age ranges between a_1 and a_2 is introduced so that both aging and apoptosis of the CCs can be considered. Therefore, $V^i(t) = \int_0^\infty v^i(a,t)da$.

Assuming biological age coincides with chronological age, the evolution of the age distribution function of the ith lineage of CC is governed by the following equations

$$\frac{\partial\, v^i(a,t)}{\partial t} + \frac{\partial\, v^i(a,t)}{\partial a} = -\mu^i(a)\; v^i(a,t) - \rho^i(a)\; v^i(a,t)\; F(P(t)) \;, \quad i = 1,2,\dots,M \;, \tag{3.3}$$

where $\mu^i(a)$ and $\rho^i(a)$ represent the mortality and the replication rate of the cells of the i-th lineage in function of their age.

Equations (3.3) are supplemented by the following initial-boundary conditions

$$v^i(a,0) = v^{i,0}(a) > 0 \;, \quad i = 1,2,\dots,M \;, \tag{3.4}$$

$$v^i(0,t) = \rho\, d^i\, F(P(t))\, U(t) + 2\int_0^\infty \rho^i(a)\, v^i(a,t)\, F(P(t))\, da \;, \quad i = 1,2,\dots,M \;, \tag{3.5}$$

The well-posedness of problem (3.1)–(3.5) is discussed in Appendix A. Moreover, we refer the interested reader to examine the McKendrick's age-structured population model [11, 39].

A special case in which functions $\rho^1(a)$ and $\mu^i(a)$ are piecewise constant are considered towards simplifying numerical calculations and comparing the model with the results of simulations based on space-dependent mechanisms and stochastic rules. Specifically, the existence of 4 age intervals $(0,a_1)$, (a_1,a_2), (a_2,a_3), (a_3,A) (newborn, juveniles, adult and senescent cells) and A being the maximum age of the cells are assumed. The values of ρ and μ are denoted by $\rho_{(1)}$, $\rho_{(2)}$, $\rho_{(3)}$, $\rho_{(4)}$ and $\mu_{(1)}$, $\mu_{(2)}$, $\mu_{(3)}$, $\mu_{(4)}$ in those intervals. Moreover, the numbers of CCs of the age classes of the i-th lineage are indicated by $V^i_{(1)}$, $V^i_{(2)}$, $V^i_{(3)}$, $V^i_{(4)}$.

Then, equation 3.3 is integrated in each age interval and equation 3.5 is considered, resulting in

$$\begin{cases} \dot V^i_{(1)}(t) = \rho d F(P(t))U(t) + \big(\rho_{(1)}V^i_{(1)}(t) + 2\rho_{(2)}V^i_{(2)}(t) + 2\rho_{(3)}V^i_{(3)}(t) + 2\rho_{(4)}V^i_{(4)}(t)\big)F(P(t)) - \\ \qquad\qquad - v^i(a_1,t) - \mu_{(1)}V^i_{(1)}(t) \;, \\ \dot V^i_{(2)}(t) = v^i(a_1,t) - v^i(a_2,t) - \rho_{(2)}V_{(2)}(t)F(P(t)) - \mu_{(2)}V^i_{(2)}(t) \;, \\ \dot V^i_{(3)}(t) = v^i(a_2,t) - v^i(a_3,t) - \rho_{(3)}V_{(3)}(t)F(P(t)) - \mu_{(3)}V^i_{(3)}(t) \;, \\ \dot V^i_{(4)}(t) = v^i(a_3,t) - \rho_{(4)}V_{(4)}(t)F(P(t)) - \mu_{(4)}V^i_{(4)}(t) \;. \end{cases} \tag{3.6}$$

The total number of CCs is given by

$$\dot V(t) = \rho\, d\, F(P(t))\, U(t) \sum_{i=1}^{M}\sum_{j=1}^{4} \rho_{(j)} V^i_{(j)}\, F(P(t)) - \sum_{j=1}^{4} \mu_{(j)} V^i_{(j)} \;. \tag{3.7}$$

Since it is usual in compartmental models, the case in which the age distribution within each class is negligible can be considered; therefore,

$$\psi_{(j)} v^i(a_j,t) = V^i_{(j)}(t) \;, \tag{3.8}$$

where $\psi_{(j)}$ measures the width of the j-th age class (or the time spent by the cell in the j-th class).

TABLE 3. Setup of parameters for the differential equations numerical simulations. In variables, the subscript stands for the age and the superscript stands for the lineage. When the superscript is not reported all the lineages have the same configuration.

CSC	Newborn CC			Juvenile CC		
$\rho = 1$	Lineage 1	Lineage 2	Lineage 3	Lineage 1	Lineage 2	Lineage 3
$d^1 = 0.2$	$\rho^1_{(1)} = 0.7$	$\rho^2_{(1)} = 0.6$	$\rho^3_{(1)} = 0.5$	$\rho^1_{(2)} = 0.9$	$\rho^2_{(2)} = 0.8$	$\rho^3_{(2)} = 0.7$
$d^2 = 0.3$	$\mu^1_{(1)} = 0.30$	$\mu^2_{(1)} = 0.33$	$\mu^3_{(1)} = 0.33$	$\mu^1_{(2)} = 0.30$	$\mu^2_{(2)} = 0.33$	$\mu^3_{(2)} = 0.33$
$d^3 = 0.3$	$\gamma_{(1)} = 1$			$\gamma_{(2)} = 1$		
–						

Adult CC			Senescent CC		
Lineage 1	Lineage 2	Lineage 3	Lineage 1	Lineage 2	Lineage 3
$\rho^1_{(3)} = 1.0$	$\rho^2_{(3)} = 0.9$	$\rho^3_{(3)} = 0.8$	$\rho^1_{(4)} = 0.5$	$\rho^2_{(4)} = 0.4$	$\rho^3_{(4)} = 0.3$
$\mu^1_{(3)} = 0.30$	$\mu^2_{(3)} = 0.33$	$\mu^3_{(3)} = 0.33$	$\mu^1_{(4)} = 0.48$	$\mu^2_{(4)} = 0.50$	$\mu^3_{(4)} = 0.50$
$\gamma_{(3)} = 1$			–		

Omitting the lineages for a further simplification of the notation and combining equations (3.1), (3.6) and (3.8), we obtain the following complete system

$$\begin{cases} \dot{U}(t) = \rho\,(1-d)\,U(t)\,F(P(t)) \\ \dot{V}_{(1)}(t) = \rho\,d\,F(P(t))\,U(t) - (\gamma_{(1)} + \mu_{(1)})\,V_{(1)}(t) \\ \qquad\quad + \Big(\rho_{(1)}V_{(1)}(t) + 2\rho_{(2)}V(2)(t) + 2\rho_{(3)}V_{(3)}(t) + 2\rho_{(4)}V_{(4)}(t)\Big)F(P(t)) \ , \\ \dot{V}_{(2)}(t) = \gamma_{(1)}V_{(1)}(t) - (\gamma_{(2)} + \mu_{(2)})\,V_{(2)}(t) - \rho_{(2)}V_{(2)}(t)F(P(t)) \ , \\ \dot{V}_{(3)}(t) = \gamma_{(2)}V_{(2)}(t) - (\gamma_{(3)} + \mu_{(3)})\,V_{(3)}(t) - \rho_{(3)}V_{(3)}(t)F(P(t)) \ , \\ \dot{V}_{(4)}(t) = \gamma_{(3)}V_{(3)}(t) - \mu_{(4)}V_{(4)}(t) - \rho_{(4)}V_{(4)}(t)F(P(t)) \ . \end{cases} \tag{3.9}$$

with $\gamma_{(j)} = 1/\psi_{(j)}$, for $j = 1, 2, 3$.

Remark 3.1. In an oversimplified case, ρ and μ are constant and the integration of equation (3.3) yields

$$\dot{V}^i(t) = \rho\,d^i\,F(P(t))\,U(t) + \rho V^i\,F(P(t)) - \mu V^i \ , \quad i = 1, 2, \ldots, M \ , \tag{3.10}$$

and summing over i hence we have the following system of ordinary differential equations (ODEs)

$$\begin{cases} \dot{V}(t) = \rho\,d\,F(P(t))\,U(t) + \rho\,V(t)\,F(P(t)) - \mu\,V(t) \ , \\ \dot{U}(t) = \rho\,(1-d)\,F(P(t))\,U(t) \ . \end{cases} \tag{3.11}$$

3.2. Numerical simulations

Problem (3.9) is numerically solved considering 3 cell lineages with `ode45` Matlab solver based on explicit Runge-Kutta method. Since the crowding effect is averaged over the entire available space, a duration of the phenomenon is naturally considered such that a large part of the entire domain can be occupied by the cells. At this point, if $U(0) > 0$, then system (3.9) has only one equilibrium state, *i.e.*, $U = 1$ and $V^i = 0$. The initial conditions are analogous to the simulations performed with CA, *i.e.*, $U(0) = 27/50^3$ and $V^i_{(j)}(0) = 0$, for all i and j. Monotonic decreasing function $F(P) = (1-P)^2$ was set in the subsequent simulations so that the crowding effect could be taken into consideration. The other parameters are listed in Table 3.

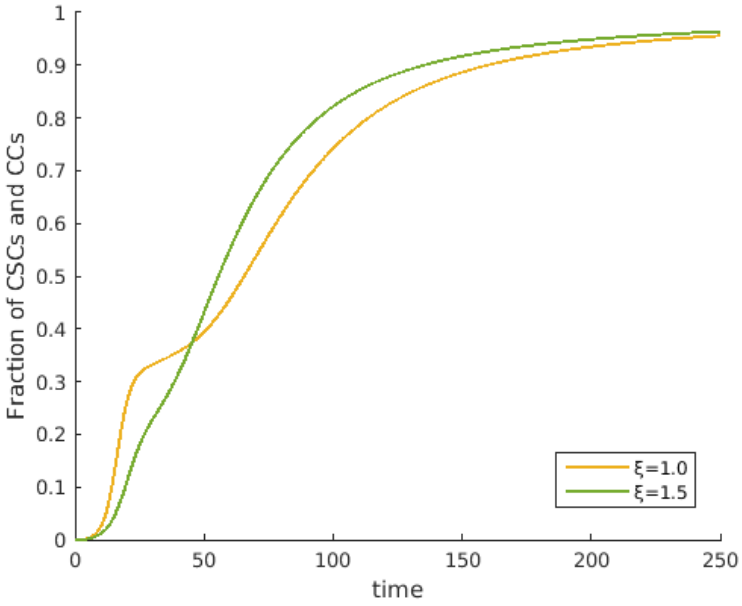

FIGURE 10. Quantitative evolution of the number of tumoral cells (CSCs and CCs) over the lattice spaces with respect to the mortality variation ($\xi = 1.0$ and $\xi = 1.5$), adopting the differential equations model. The initial conditions are $U(0) = 27/50^3$ and $V^i_{(j)}(0) = 0$, for all i and j. Parameters are listed in Table 3.

Similarly to the case with cellular automata, the behaviour of the system is studied with respect to the variation in mortality tuning the values of the last parameter with multiplicative factor ξ. Figure 10 displays the graphs of the total (CSCs and CCs of all ages and lineages) volume fraction of the tumour. Again, the tumour growth paradox occurs. Let us observe the phenomenon in detail in Figure 11, considering once again, what happens at the level of age classes and lineages, choosing the mortality setting ξ equal to 1.0 and 1.5.

In the case of a lower mortality, the initial phase of tumour evolution shows a greater crowding of CCs (panels (a), (b), and (c)), in particular with respect to the lineage 1 (panel (a)). In the case with a higher mortality (which could be induced by medical treatment), the progression of the disease seems to initially benefit from a significant lowering of the CCs (panels (d), (e), and (f)). However, this same event also results to be not positive over time. Again, the differential equations model also suggests that the presence of CCs contributes to limiting an accelerated tumour growth induced by CSCs.

3.3. Differential equations vs. CA models

The introduction of a function F to take into account for the competition for space was suggested for the first time in the seminal paper [20]. This seems to be a heuristic way of approaching the problem since competition is clearly a local effect, whereas multiplying the replication rate by $F(P)$ affects equally every cell of the system. Nevertheless, it proves to be an useful shortcut to avoid time-consuming simulations based on agent-based methods in some cases. As an example, let us consider the plots of Figure 12 where the time evolution of the total number of tumoural cells in the given lattice $50 \times 50 \times 50$ is shown. We have considered the same setup of parameters (Tabs. 1 and 2 for the 3 lineages of CCs) of simulation of Figure 6 with $\xi = 1.0$. Initially, there are 1000 CSCs and four different initial situations are considered: cells that are initially uniformly distributed over the grid, or cells that are initially divided in 1, 2, or 8 blocks. These limit cases show the importance of using numerical methods that include space dependence whereas models of differential equations based on an "averaged" crowding effect cannot be used in general if spatial inhomogeneity is relevant.

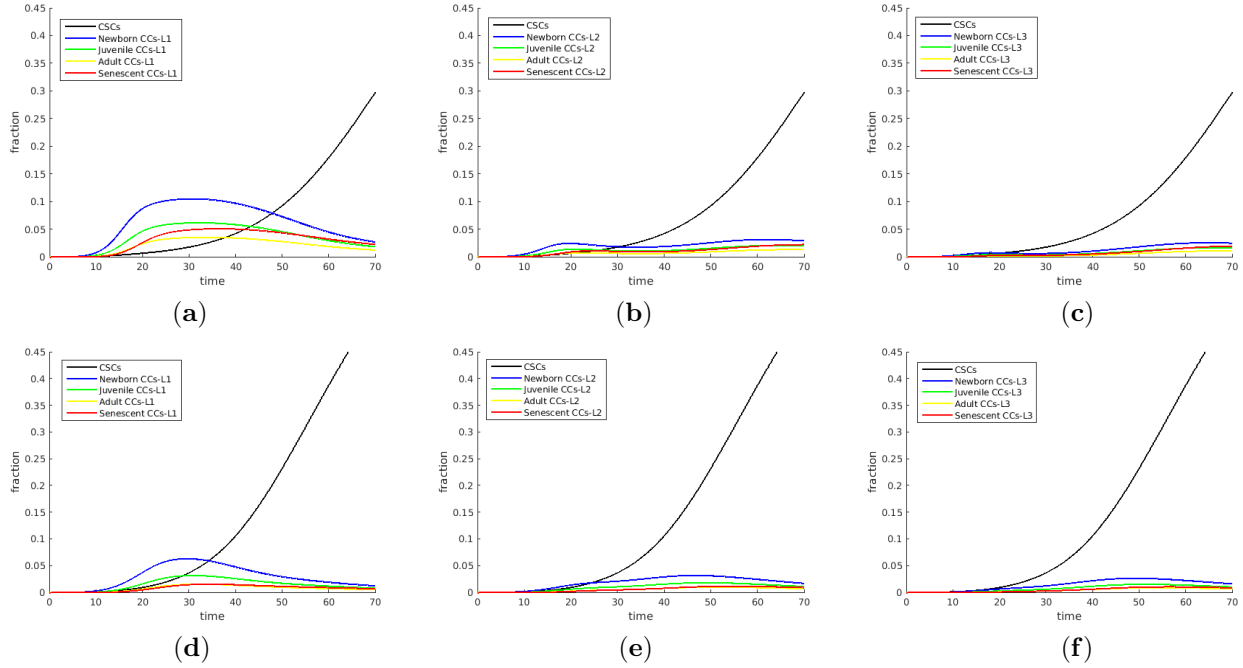

FIGURE 11. Quantitative cancer progression according to age class and lineage. The panels (a), (b) and (c) show the results for a mortality value resulting from $\xi = 1.0$, while the panels for (d), (e) and (f) concern the simulations with $\xi = 1.5$. In the legends L1, L2 and L3 stand for first, second and third lineage, respectively. The simulation is the same of Figure 10.

Nevertheless, it can be seen experimentally that the solution obtained by CA can be easily approximated by compartmental models if a particular form of $F(P)$ is chosen, to fit the particular class of problems that are considered.

For example, let us consider the first case illustrated in Figure 12 (initially, uniformly distributed cells). It can be seen (Fig. 13) that the system of differential equations fits satisfactorily the solution found with CA if $F(P)$ is taken equal to $(1-P)^\eta$, with $\eta = 1$. Comparing Figure 12 with Figure 13, we can observe that the exponent $\eta = 2$ allows to fit better cases with inhomogeneous initial conditions. The results of Figure 13 were obtained by solving the equations of the system 3.9, with the parameters of Table 3 and $\xi = 1.0$, and setting the initial conditions $U(0) = 1000/50^3$ and $V^i_{(j)}(0) = 0$, for all i and j.

We add a final comment. According to Remark 2.2, throughout the CA model we have considered as the neighborhood of a would-be mother cell a cubic domain of $3 \times 3 \times 3$ cells where a newborn cell can be generated. One can ask if the CA model (even with an unfavorable initial condition, such as the case of a centralized mass of CSCs) approximates the results of the model based on differential equations with $F(P) = 1 - P$ when the dimensions of the neighborhood are increased. The results of CA simulations using different sizes of neighborhood are shown in Figure 14. The test are performed with the same setup of Tables 1 and 2 and $\xi = 1.0$. We set 1000 CSCs in the center of lattice as initial condition. As we can observe from the graphs, as the size of the neighborhood increases, the curves tend towards the solution of the differential model with $F(P) = 1 - P$. In particular, the purple curve (neighborhood $15 \times 15 \times 15$) is a good approximation of the black one, corresponding of the solution of ODEs system 3.9 with $F(P) = 1 - P$.

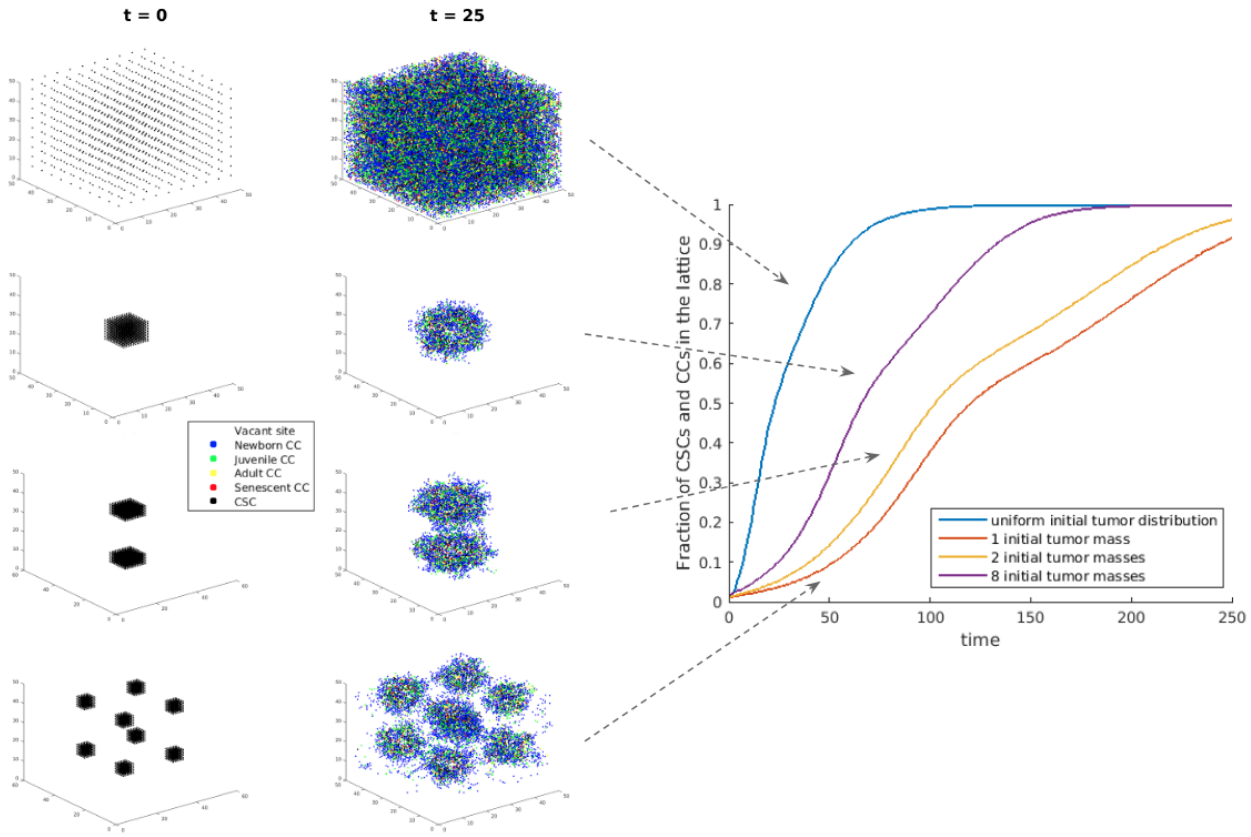

FIGURE 12. CA simulations for different initial distributions. The parameters setup is provided in Table 1 for the CSCs, in Table 2 for the 3 lineages of CCs, and with $\xi = 1.0$. The initial condition of 1000 CSCs uniformly distribuited or separeted in 1, 2, 8 masses are displayed on the left-side (under $t = 0$). We report also the panels of the system evolution at time $t = 25$. On the right-site, the graph concerns the quantitative evolution (averaged over 10 test) of the fraction of tumoral cells (CSCs and CCs).

4. Conclusions

This article presented and discussed a conceptual model for the growth of tumours in the presence of CSCs and several lineages of ordinary CCs, assuming mitosis can be hindered by the crowding of cells. Aging and apoptosis of CCs were also taken into account.

The model was implemented in the framework of 3D cellular automata, where the rules governing the evolution of CA are expressed in terms of stochastic dynamics. The development of the tumour mass can be simulated as well as the evolution of the different lineages and age classes of CCs.

The model exhibits the so-called tumour growth paradox, *i.e.*, the fact that the speed of the tumour growth can be greater when the mortality of the CCs increases. Examples in which cytotoxic intervention exerts a counterproductive effect were provided. The same paradoxical effect occurs as well when the rate of replication of CCs is artificially reduced, a fact that was not considered in the existing literature on tumour growth paradox.

A deterministic model was also introduced and studied in which the unknown functions to be determined are the total number of CSCs and the age distribution of each lineage of CC. Since this approach neglects space dependence, the crowding effect cannot be modeled as a local effect but its influence is modeled assuming

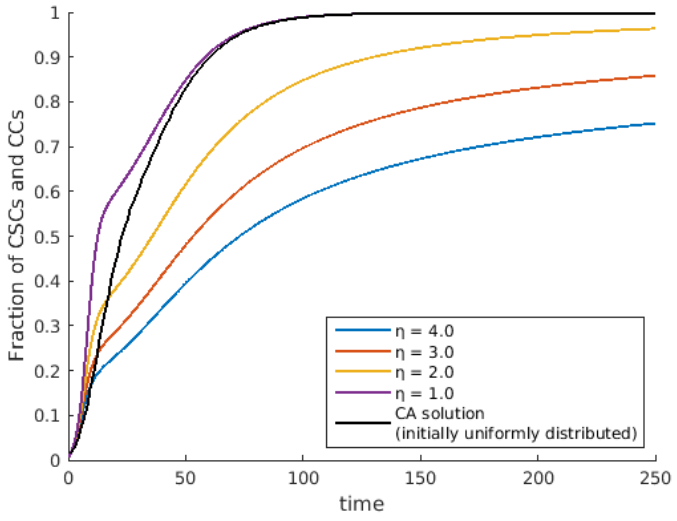

FIGURE 13. Quantitative time evolution of the number of tumoral cells (CSCs and CCs) solving the differential equations model 3.9, for different choices of $F(P) = (1-P)^{\eta}$. Parameters are listed in Table 3 and $\xi = 1.0$. The initial conditions are $U(0) = 1000/50^3$ and $V^i_{(j)}(0) = 0$, for all i and j. Is is also displayed the curve (in black colour) corresponding to the solution of the CA model with initially uniformly distributed CSCs, as simulation of Figure 12.

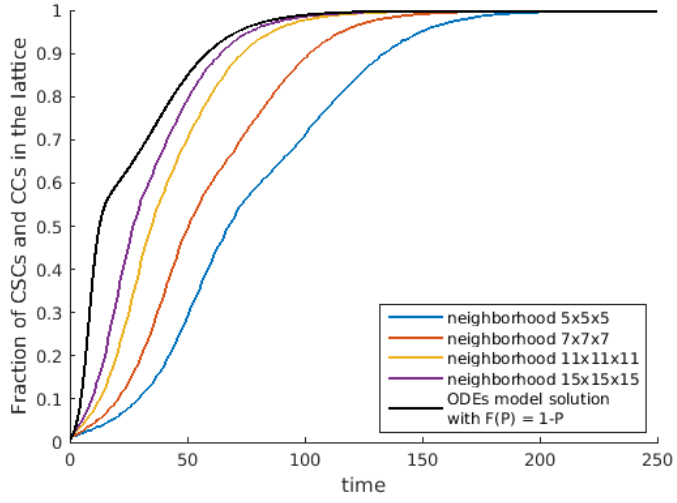

FIGURE 14. Quantitative time evolution of the number of tumoral cells (CSCs and CCs) performing CA simulations for different size of neighborhood. The parameters are listed in Table 1 and in Table 2 for the 3 lineages of CCs, and $\xi = 1.0$. The initial condition is a central mass of 1000 CSCs. Is is also displayed the curve (in black colour) corresponding to the solution of the differential equations model (system 3.9) with $F(P) = 1 - P$, as computed Figure 13.

that the rate of reproduction of the cells is reduced as a function $F(P)$ of the fraction of the volume of the tumour with reference to to the total available volume. The mathematical model is a non-standard system of first order ordinary and partial differential equations whose well-posedness is proved in an Appendix. Numerical simulations were made using the same values for the parameters as in the case of the CA model. We showed that the two classes of models give the same qualitative results (including the tumour growth paradox) and that the plots of the evolution of the tumoural mass over time are in agreement when the initial conditions are sufficiently homogeneous in space and for properly chosen function $F(P)$. As expected, the two models differ when the initial condition is such that the cells are concentrated in a small portion of the available volume, but that the difference tends to decrease when the "local crowding" modelled in the CA scheme concerns a larger neighborhood of the replicating cell.

As we pointed out in the Introduction, the models presented and discussed here extend the validity of the results presented in recent literature since they can be applied to cases of 3D and to tumours with several lineages of differentiated cancer cells and take into account the variability of the parameters of the cells with their age. Moreover, we showed that also a decreased reproduction rate of CCs can paradoxically lead to accelerated tumour growth. Finally, it is of some interest the comparison of the simulations based on individual cell description and of computations based on quantities averaged over the available space.

Appendix A. Well-posedness of problem (3.1)–(3.5)

We aim to prove the well-posedness (existence and uniqueness of a solution whose value depends continuously on data) of problem (3.1)–(3.5) in a time interval (O,T). With no lack of generality and towards simplifying notation, the case of only one lineage of CCs will be treated in 2 steps. First, an auxiliary problem will be introduced for proving it has a unique solution. The result will used to solve the main problem.

Step 1. For any prescribed function $\Psi(t)$, $0 \le \Psi(t) \le 1$, with Lipschitz constant K in $[0,T]$, the following auxiliary problem is solved:

$$\begin{cases} v_a + v_t = h(a,t)\, v \ , & a \in (0,A) \ , \ t \in (0,T) \ , \\ v(a,0) = v_0(a) \ , & a \in (0,A) \ , \\ v(0,t) = \Phi(t) + 2\Psi(t) \int_0^A \rho(a) v(a,t) da \ , & t \in (0,T) \ , \end{cases} \tag{A.1}$$

where

$$h(a,t) = -\mu(a) - \rho(a)\ \Psi(t), \qquad a \in (0,A) \ , \ t \in (0,T) \ , \tag{A.2}$$

$$\Phi(t) = \rho_0\, d\, \Psi(t)\, U_0 \exp\left[\rho_0 (1-d) \int_0^t \Psi(t)(\tau) d\tau\right] , \qquad t \in (0,T) \ . \tag{A.3}$$

Concerning the initial data, it is assumed that

H1 $U_0 > 0$[4],

H2 $v_0(a)$ is a continuous non-negative function with support in $(0,\alpha)$ and such that $U_0 + \int_0^\alpha v_0(a)\, da \ \le \ 1$.

Finally, $A = \alpha + T$ is taken in (A.1).

Proposition A.1. *Under hypotheses (H1)–(H2), the auxiliary problem (A.1)–(A.3) is well-posed, having a unique solution.*

[4]Case $U_0 = 0$ corresponds to the trivial case in which no CSCs are present.

Proof of Proposition A.1. A fixed point argument is used to solve problem (A.1)–(A.3) and a non-negative function $X(t) \in C^1(0,T)$ is assigned such that

$$0 \le X(t) \le K_1 \ , \qquad | \, \dot{X}(t) \, | \le K_2 \ , \tag{A.4}$$

(where K_1 and K_2 are constants to be chosen). The following linear problem is solved:

$$\begin{cases} v_a + v_t = h(a,t)\, v \ , & a \in (0,A) \ , \ t \in (0,T) \ , \\ v(a,0) = v_0(a) \ , & a \in (0,A) \ , \\ v(0,t) = \Phi(t) + 2\Psi(t) X(t) \ , & t \in (0,T) \ . \end{cases} \tag{A.5}$$

Since the data are non-negative and bounded and $h(a,t)$ is non-positive, $v(a,t)$ is non-negative and bounded in $(0\,,\ A) \times (0\,,T)$. Defining

$$\widetilde{X}(t) = \int_0^A \rho(a) v(a,t) da \ , \qquad t \in (0,T) \ , \tag{A.6}$$

where $v(a,t)$ is the solution to problem (A.5), we obtain a mapping $\mathcal{T}$

$$\widetilde{X}(t) = \mathcal{T}\, X(t) \ , \qquad t \in (0,T) \ . \tag{A.7}$$

Since $v(a,t)$ vanishes for $\alpha + t < a < A$, $0 < t < T$, then

$$\widetilde{X}(t) = \int_0^t \rho(a)\, v(a,t)\, da + \int_t^{\alpha+t} \rho(a)\, v(a,t)\, da \ . \tag{A.8}$$

Clearly, $\widetilde{X}(t)$ in non-negative. Moreover, the second term is bounded by a constant $B = A \max \rho$, whereas the first (the only one depending on $X(t)$) is $O(t)$. Therefore, choosing *e.g.* $K_1 = 2B$, T can be determined so that

$$0 \le \widetilde{X}(t) \le K_1 \ . \tag{A.9}$$

In addition, it is

$$| \, \dot{\widetilde{X}}(t) \, | \le \max \rho \left[\int_0^A \left| \frac{\partial v}{\partial t} \right| da \right] \ = \ \max \rho \left[\int_0^t \left| \frac{\partial v}{\partial t} \right| da \ + \ \int_t^{\alpha+T} \left| \frac{\partial v}{\partial t} \right| da \right]. \tag{A.10}$$

The second term in the r.h.s of (A.10) does not contain X and $\dot{\widetilde{X}}$ is bounded by a constant C, while the first term is $O(t)$. Therefore, choosing *e.g.*, $K_2 = 2C$, a value T can be determined so that the r.h.s. of (A.10) is dominated by K_2 and thus $\mathcal{T}$ maps the set defined by (A.4) into itself.

Next, the uniform norm of $\widetilde{X}_1 - \widetilde{X}_2$ must be evaluated where, for $i = 1, 2$ it is $\widetilde{X}_i = \int_0^A \rho(a)\, v_i(a,t)\, da$ and $v_i(a,t)$ is the solution to problem (A.5) with boundary datum

$$v_i(0,t) = \Phi(t) + 2\Psi(t) X_i(t) \ , \qquad t \in (0,T) \ .$$

As a result,

$$| \, \widetilde{X}_1(t) - \widetilde{X}_2(t) \, | \le \max \rho \int_0^t | \, v_1(a,t) - v_2(a,t) \, | \, da \ .$$

In turn, difference $\mid v_1(a,t) - v_2(a,t) \mid$ can be estimated in terms of difference of the boundary data. Consequently, reducing T, if necessary, the transformation is a contraction and the Banach fixed point theorem ensures $\mathcal{T}$ has a unique fixed point. Consequently, problem (A.1)–(A.3) has a unique solution. □

Step 2. The previous result is used to prove the following theorem.

Theorem A.2. *Problem (3.1)–(3.5) is well-posed in a suitable domain* $(0\,,\ A) \times (0\,, T)$.

Proof of Theorem A.2. Similarly to the previous case of Proposition A.1, a fixed point technique will be adopted. For a given function $p(t) \in C^1(0,T)$, such that

$$0 < P_1 \le p(t) \le P_2\ , \qquad \mid \dot{p}(t) \mid < P_3\ , \tag{A.11}$$

function $\Psi(t) = F(p(t))$ is defined. Then, with the choice of $\Psi(t)$ problem (A.1)–(A.3) is solved, as in Step 1, obtaining a function $v(a,t)$. We define

$$\widetilde{p}(t) = U_0\, \exp[\rho\,(1-d) \int_0^t F(p(\tau))\, d\tau] + \int_0^A v(a,t) da. \tag{A.12}$$

Also in this case, the only term dependent on p is $O(t)$; therefore, if the second integral is denoted by I, it is sufficient to choose $P_1 = I/2$ and $P_2 = 2I$ to conclude $p(t)$ satisfies the first inequality in (A.11). Moreover, it is

$$\dot{\widetilde{p}}(t) = U_0\, \exp[\rho\,(1-d) \int_0^t F(p(\tau))\, d\tau] F(p(t)) + \int_0^A \frac{\partial v}{\partial t}(a,t)\, da, \tag{A.13}$$

and, therefore, $\dot{\widetilde{p}}(t)$ is bounded independently of $\widetilde{p}(t)$. The third inequality in (A.11) holds for $\widetilde{p}(t)$, meaning transformation $\mathcal{P}$ defined by (A.13) maps set (A.11) into itself. Consequently, T can be chosen so that $\mathcal{P}$ is a contraction. Indeed

$$\mid \widetilde{p}_1(t) - \widetilde{p}_2(t) \mid = \ U_0 \ \left| \exp[\rho\,(1-d) \int_0^t F(p_1(\tau))\, d\tau] - \exp[\rho\,(1-d) \int_0^t F(p_2(\tau))\, d\tau] \right|$$

$$+ \int_0^A \mid v_1(a,t) - v_2(a,t) \mid da.$$

The first term is estimated in term of $\mid p_1 - p_2 \mid O(t)$ because of the Lipschitz continuity of F. The integral in the second term can be splitted

$$\int_0^A \mid v_1(a,t) - v_2(a,t) \mid da = \int_0^t \mid v_1(a,t) - v_2(a,t) \mid da + \int_t^A \mid v_1(a,t) - v_2(a,t) \mid da.$$

Functions v_i $(i = 1,2)$ solve problem (A.1)–(A.3), in which the boundary datum is given by $\Phi(t) + 2\Psi(t) \int_0^A \rho(a) v(a,t)\ da$ and the r.h.t. in (A.1) is given by $h_i(a,t)\, v = -[\mu(a) + \rho(a)\Psi_i(t)]\, v$. In the second term, the initial data of v_1 and v_2 are equal and the difference is estimated in terms of the integral of $\mid h_1 - h_2 \mid$, hence $\mid F(p_1(\tau)) - F(p_2(\tau)) \mid\ O(t)$. The integrand of the first term is estimated in terms of difference in the boundary data plus the integral of $\mid h_1 - h_2 \mid$. Therefore, the first term is $\mid p_1 - p_2 \mid\ O(t)$ and T can be chosen so that $\mid \widetilde{p}_1 - \widetilde{p}_2 \mid < \beta \mid p_1 - p_2 \mid$ with $\beta < 1$. Using again the Banach fixed point theorem, the proof of the well-posedness of problem (3.1) – (3.5) is finally concluded. □

Acknowledgements. This research was funded by INCT-MACC (Instituto Nacional de Ciência e Tecnologia - Medicina Assistida por Computação Científica), approved by CNPq (Conselho Nacional de Desenvolvimento Científico e

Tecnológico) of Brazil, and financed by FAPESP (Fundação de Amparo à Pesquisa do Estado de São Paulo) of Brazil (Grant 2014/50889-7). L.M. acknowledges CAPES (Coordenação de Aperfeiçoamento de Pessoal de Nível Superior), from the Ministry of Education of Federal Republic of Brazil, for the financial support provided (Grant PROEX-9740044/D). A sincere thank you to Prof. Angela Cristina Pregnolato Giampedro of PUSP-SC (Prefeitura do Campus USP de São Carlos) for her proofreading of this manuscript.

References

[1] A. Anderson, M.A.J. Chaplain and K. Rejniak, Single-cell-based models in biology and medicine. Springer Science & Business Media (2007).

[2] E.C. Anderson, C. Hessman, T.G. Levin, M.M. Monroe and M.H. Wong, The role of colorectal cancer stem cells in metastatic disease and therapeutic response. *Cancers* **3** (2011) 319–339.

[3] E. Beretta, V. Capasso and N. Morozova, Mathematical modelling of cancer stem cells population behavior. *Math. Modell. Natur. Phenomena* **7** (2012) 279–305.

[4] E. Beretta, N. Morozova, V. Capasso and A. Harel-Bellan, Some results on the population behavior of cancer stem cells. In *New Challenges for Cancer Systems Biomedicine*. Springer (2012), pp. 145–172.

[5] R. Betteridge, M.R. Owen, H.M. Byrne, T. Alarcón and P.K. Maini, The impact of cell crowding and active cell movement on vascular tumour growth. *Netw. Heterogene. Media* **1** (2006) 515.

[6] A. Boondirek, W. Triampo and N. Nuttavut, A review of cellular automata models of tumor growth. In *Int. Math. Forum* **5** (2010) 3023–3029.

[7] I. Borsi, A. Fasano, M. Primicerio and T. Hillen, Mathematical properties of a non-local integro-PDE model for cancer stem cells. *Math. Med. Biol.* **34** (2015) 59–75.

[8] R.W. Cho and M.F. Clarke, Recent advances in cancer stem cells. *Curr. Opin. Genetics Dev.* **18** (2008) 48–53.

[9] M.F. Clarke and M. Fuller, Stem cells and cancer: two faces of eve. *Cell* **124** (2006) 1111–1115.

[10] H. Clevers, The cancer stem cell: premises, promises and challenges. *Nat. Med.* **17** (2011) 313–319.

[11] G. De Vries, T. Hillen, M. Lewis, J. Müller and B. Schönfisch, *A course in mathematical biology: quantitative modeling with mathematical and computational methods*. SIAM (2006).

[12] H. Enderling, A.R. Anderson, M.A. Chaplain, A. Beheshti, L. Hlatky and P. Hahnfeldt, Paradoxical dependencies of tumor dormancy and progression on basic cell kinetics. *Cancer Res.* **69** (2009) 8814–8821.

[13] H. Enderling and P. Hahnfeldt, Cancer stem cells in solid tumors: Is 'evading apoptosis a hallmark of cancer*Progr. Biophys. Molec. Biol.* **106** (2011) 391–399.

[14] A. Fasano, A. Mancini and M. Primicerio, Tumours with cancer stem cells: a PDE model. *Math. Biosci.* **272** (2016) 76–80.

[15] F. Forouzannia, H. Enderling and M. Kohandel, Mathematical modeling of the effects of tumor heterogeneity on the efficiency of radiation treatment schedule. *Bull. Math. Biol.* **80** (2018) 283–293.

[16] R. Ganguly and I. Puri, Mathematical model for the cancer stem cell hypothesis. *Cell Proliferat.* **39** (2006) 3–14.

[17] X. Gao, J.T. McDonald, L. Hlatky and H. Enderling, Cell–cell interactions in solid tumors – the role of cancer stem cells. In *New Challenges for Cancer Systems Biomedicine* (Springer, 2012), pp. 191–204

[18] K.V. Gurova and A.V. Gudkov, Paradoxical role of apoptosis in tumor progression. *J. Cell. Biochem.* **88** (2003) 128–137.

[19] M. Hadjicharalambous, P.A. Wijeratne and V. Vavourakis, From tumour perfusion to drug delivery and clinical translation of in silico cancer models. *Methods* **185** (2021) 82–93.

[20] T. Hillen, H. Enderling and P. Hahnfeldt, The tumor growth paradox and immune system-mediated selection for cancer stem cells. *Bull. Math. Biol.* **75** (2013) 161–184.

[21] B.J. Huntly and D.G. Gilliland, Summing up cancer stem cells. *Nature* **435** (2005) 1169–1170.

[22] M. Marzagalli, F. Fontana, M. Raimondi and P. Limonta, Cancer stem cells – key players in tumor relapse. *Cancers* **13** (2021) 376.

[23] L. Meacci, D. de Oliveira Medeiros, G. Buscaglia and M. Primicerio. O paradoxo do crescimento tumoral atraves de um modelo 3d de automatos celulares com celulas– tronco cancerıgenas. *CQD–Revista Eletronica Paulista de Matematica* **14** (2019) 132–146.

[24] L. Meacci and M. Primicerio, Mathematical models for tumours with cancer stem cells. *Comput. Appl. Math.* **37** (2018) 6544–6559.

[25] L. Meacci, M. Primicerio and G.C. Buscaglia, Growth of tumours with stem cells: The effect of crowding and ageing of cells. *Physica A* **570** (2021) 125841.

[26] J. Metzcar, Y. Wang, R. Heiland and P. Macklin, A review of cell-based computational modeling in cancer biology. *JCO Clin. Cancer Inf.* **2** (2019) 1–13.

[27] F. Michor *et al.*, Mathematical models of cancer stem cells. *J. Clin. Oncol.* **26** (2008) 2854–2861.

[28] R. Molina-Peña and M.M. Álvarez, A simple mathematical model based on the cancer stem cell hypothesis suggests kinetic commonalities in solid tumor growth. *PloS One* **7** (2012) e26233.

[29] R. Molina-Peña, J.C. Tudon-Martinez and O. Aquines-Gutiérrez, A mathematical model of average dynamics in a stem cell hierarchy suggests the combinatorial targeting of cancer stem cells and progenitor cells as a potential strategy against tumor growth. *Cancers* **12** (2020) 2590.

[30] Á. Monteagudo and J. Santos, Studying the capability of different cancer hallmarks to initiate tumor growth using a cellular automaton simulation. Application in a cancer stem cell context. *Biosystems* **115** (2014) 46–58.
[31] Á. Monteagudo and J. Santos, Treatment analysis in a cancer stem cell context using a tumor growth model based on cellular automata. *PloS ONE* **10** (2015) e0132306.
[32] T. Nunes, D. Hamdan, C. Leboeuf, M. El Bouchtaoui, G. Gapihan, T.T. Nguyen, S. Meles, E. Angeli, P. Ratajczak, H. Lu et al, Targeting cancer stem cells to overcome chemoresistance. *Int. J. Molec. Sci.* **19** (2018) 4036.
[33] J. Poleszczuk and H. Enderling, A high-performance cellular automaton model of tumor growth with dynamically growing domains. *Appl. Math.* **5** (2014) 144.
[34] M. Prieto-Vila, R.-u. Takahashi, W. Usuba, I. Kohama and T. Ochiya, Drug resistance driven by cancer stem cells and their niche. *Int. J. Mol. Sci.* **18** (2017) 2574.
[35] T. Reya, S.J. Morrison, M.F. Clarke and I.L. Weissman, Stem cells, cancer, and cancer stem cells. *Nature* **414** (2001) 105–111.
[36] A. Rivaz, M. Azizian and M. Soltani, Various mathematical models of tumor growth with reference to cancer stem cells: a review. *Iran. J. Sci. Technol. Trans. A* **43** (2019) 687–700.
[37] M.W. Schmitt, M.J. Prindle and L.A. Loeb, Implications of genetic heterogeneity in cancer. *Ann. New York Acad. Sci.* **1267** (2012) 110.
[38] A. Shyntar, A. Patel, M. Rhodes, H. Enderling and T. Hillen, The tumor invasion paradox in cancer stem cell-driven solid tumors. *Bull. Mathemat. Biol.* **84** (2022) 1–24.
[39] H.R. Thieme, Vol. 12 of *Mathematics in population biology*. Princeton University Press (2018).
[40] C. Tomasetti, L. Li and B. Vogelstein, Stem cell divisions, somatic mutations, cancer etiology, and cancer prevention. *Science* **355** (2017) 1330–1334.
[41] C. Tomasetti, B. Vogelstein and G. Parmigiani, Half or more of the somatic mutations in cancers of self-renewing tissues originate prior to tumor initiation. *Proc. Natl. Acad. Sci.* **110** (2013) 1999–2004.
[42] J.E. Visvader and G.J. Lindeman, Cancer stem cells in solid tumours: accumulating evidence and unresolved questions. *Nat. Rev. Cancer* **8** (2008) 755–768.
[43] S.L. Weekes, B. Barker, S. Bober, K. Cisneros, J. Cline, A. Thompson, L. Hlatky, P. Hahnfeldt and H. Enderling, A multicompartment mathematical model of cancer stem cell-driven tumor growth dynamics. *Bull. Math. Biol.* **76** (2014) 1762–1782.
[44] L.D. Weiss, N.L. Komarova and I.A. Rodriguez-Brenes, Mathematical modeling of normal and cancer stem cells. *Curr. Stem Cell Rep.* **3** (2017) 232–239.
[45] L.D. Weiss, P. van den Driessche, J.S. Lowengrub, D. Wodarz and N.L. Komarova, Effect of feedback regulation on stem cell fractions in tissues and tumors: understanding chemoresistance in cancer. *J. Theor. Biol.* **509** (2021) 110499.
[46] D. Wodarz and N. Komarova, Can loss of apoptosis protect against cancer? *Trends Genet.* **23** (2007) 232–237.